Measurement of the Junction Temperature of Light-Emitting Diodes Based on the Thermographic Measurement of the Case Temperature

Krzysztof Dziarski
Poznań University of Technology, Institute of Electric Power Engineering, Piotrowo 3A, 60-965 Poznań, Poland
Arkadiusz Hulewicz
Poznań University of Technology, Institute of Electrical Engineering and Electronics, Piotrowo 3A, 60-965 Poznań, Poland

Abstract: The article describes an indirect infrared thermographic method for measuring the junction temperature of the selected light-emitting diodes (LEDs). It presents the measurement methodology that enables a reliable assessment of this temperature. The finite element method (FEM) used in simulation work is also described. The article addresses the process of determining the coefficient values required for the simulations. It presents the results of simulation work conducted in the SolidWorks environment, the infrared thermographic measurements of the package temperature of the tested LEDs and the corresponding estimated junction temperature values. The reliability of the obtained results was confirmed using the electrical method and measurements with a Pt 1000 sensor.

Keywords: thermography, light emitting diode, metrology

1. Introduction

The noticeable increase in the popularity of LEDs (Light Emitting Diodes) is associated with the growing demand for the energy-efficient light sources. Light-emitting diodes are now widely used in residential lighting, the automotive industry and the industrial applications. They are composed of semiconductors joined in a p-n structure, referred to in this study as the junction, along with a carrier layer, a case (a transparent plastic dome) and electrodes. The advantages of LEDs include their high efficiency and long service life. As semiconductor components, their parameters are temperature dependent.

As the junction temperature increases, the slope of the LED's forward current–voltage characteristic ($I_F = f(V_F)$) changes. Consequently, with rising junction temperature (T_j), the forward voltage (V_F) of the LED decreases [1]. Other effects of operating an LED at an improper T_j value include the reduced luminous efficiency, a shift in light color (chromatic shift), and accelerated aging processes [2]. Prolonged operation at excessively high T_j may result in damage to the junction. For this reason, information about the value of T_j is crucial.

Autor korespondujący:
Krzysztof Dziarski, Krzysztof.dziarski@put.poznan.pl

Artykuł recenzowany
nadesłany 11.06.2025 r., przyjęty do druku 13.10.2025 r.

Several groups of methods for determining the junction temperature (T_j) have been described in the literature [3, 4]. The first group includes methods based on the known relationship between T_j and the Temperature Sensitive Parameter (TSP). Methods in this category are described in the JESD51 standard [22]. Parameters such as forward voltage (V_F), dynamic resistance (R_d), the junction capacitance (C_j) and the threshold voltage (V_{th}) can be used as TSPs. The relationship between T_j and TSP is specific to each individual device [3], which is one of the major drawbacks of these methods. Additionally, their application requires placing the diode in a measurement circuit, making real-time measurement impossible.

Another group of methods consists of contact methods. These can be further divided into direct and indirect methods. The direct methods are invasive techniques. Their use requires opening the package and gaining the direct access to the junction [3]. For this reason, their application is difficult and results in irreversible damage to the diode

The indirect methods consist of two stages. In the first stage, the temperature of the diode package is measured. This can be done using a temperature sensor (indirect contact methods) or a thermographic camera or pyrometer (indirect non-contact methods) [3, 5, 6]. The second stage involves determining the relationship between the case temperature T_c and the junction temperature T_j. Using a thermographic camera minimizes the risk of the electric shock during measurement. Additionally, it eliminates issues related to the unknown thermal resistance R_{th} between the temperature sensor and the package [7].

The indirect methods consist of two stages. In the first stage, the case temperature of the diode is measured. This measurement can be performed using a temperature sensor (indirect

contact methods) or with a thermographic camera or pyrometer (indirect non-contact methods) [3, 5, 6]. The second stage involves determining the relationship between the case temperature T_c and the junction temperature T_j. The use of a thermographic camera significantly reduces the risk of the electric shock during measurement. Moreover, it eliminates the issue of unknown thermal resistance R_{th} between the temperature sensor and the case [7].

Several attempts to perform the indirect thermographic junction temperature measurements can be found in the literature. In [8], the focus was on conducting thermographic measurements of the diode surface temperature which were then used to estimate the temperature distribution. In publication [9], the authors carried out an indirect thermographic measurement of the junction temperature T_j, focusing on precise the thermal imaging of the diode's case temperature T_c and on determining the relationship between T_j and T_c. Simplified thermal models were used for this purpose. A similar approach was applied in [10], where high-power LED modules were studied. The fundamentals of the thermal design for LEDs and the Finite Element Method (FEM) are discussed in the book [11]. In publication [12], the authors developed a three-dimensional thermal model of an LED, using a thermographic camera to measure the temperature distribution on the LED surface. Additionally, the thermographic measurements were compared with FEM simulation data and thermocouple measurements. In these studies, thermocouples were used to validate the thermographic measurements. They were placed as close as possible to the junction, but outside the case.

The authors are not aware of any studies comparing the results of the indirect thermographic junction temperature measurements with those obtained using electrical methods. For this reason, it was decided to conduct the research aimed at performing an indirect thermographic measurement of the LED junction temperature and comparing the result with that obtained using the electrical method. The forward voltage V_F was used as the Temperature Sensitive Parameter (TSP).

2. Methodology

2.1. Thermographic measurement of the surface temperature of the LED case

The first stage of the indirect thermographic measurement of the LED junction temperature (T_j) is the thermographic measurement of the case temperature (T_c). For the purpose of the study, five different models of 5 mm diameter Light Emitting Diodes (LEDs) were arbitrarily selected. These LEDs differed in emitted light color, the optoelectronic characteristics, and operating parameters. The basic parameters of the selected LEDs are presented in Table 1 [23–26].

The emissivity of the LED diode surface is unknown. For this reason, a reference marker was applied to the case surface of each diode using Velvet Coating 811-21, characterized by a well-defined emissivity coefficient ε, ranging from 0.970 to 0.975 within the temperature interval of 237.15 K to 355.15 K. The associated uncertainty in the emissivity value was estimated at 0.004 [13]. Next to the marker, a Pt 1000 sensor in an SMD 0603 package was placed [27]. The sensor was bonded using WLK 5 thermal adhesive (Fischer Elektronik, Lüdenscheid, Germany), known for its thermal conductivity of 0.836 W/m · K in the temperature range of 217.15 K to 422.15 K [28]. The resistance of the sensor was measured using the four-wire method. During the measurement, a current of 101.6 µA flowed through the sensor. Based on the conducted tests, it was found that a current of such intensity does not cause self-heating of the sensor.

A current I_H in the range of 5 mA to 30 mA flowed through the junction of the semiconductor diode. The flow of I_H through the junction caused an increase in the junction temperature T_j. Simultaneously, a current I_m with a value of 100 µA also flowed

Nomenclature

α – coefficient of the expansion
$\beta()$ – Dirac delta
ΔT_{cs} – change in the case temperature value obtained from the simulation
$\Delta_{grTcPt1000}$ – limit error of the case temperature value measured by Pt 1000
$\Delta_{grTccam}$ – limit error of the case temperature value obtained from thermographic measurement
ε – emissivity
$\Theta_{1/2}$ – half angle
η_o – optical efficiency
λ – wavelength of emitted radiation
λ_0 – selected wavelength at which the energy is concentrated
φ_e – radiant flux
φ_v – luminous flux
ψ – dynamic air viscosity
ω – solid angle of the beam
LER – luminous efficacy of the radiation
B_λ – normalized spectral power distribution
C_j – junction electrical capacitance
c_{th} – thermal capacity per cubic meter
e_{lam}, e_{turb}, f_{lam}, f_{turb} – coefficients
h_c – convection coefficient
h_r – radiation coefficient
I_F – forward current
I_H – heating current
I_m – measurement current
I_v – luminous intensity
k – thermal conductivity
K_m – photopic luminous efficacy constant, 683 lm/W
P_c – total power applied to the heat source
P_j – electrical power dissipated in junction
P_h – heat power
P_o – optical power
R_d – dynamic resistance
R_{th} – thermal resistance
T – temperature
$T_{c\ cam}$ – case temperature value obtained from thermographic measurement
T_{cs} – case temperature value obtained from the simulation
T_c – case temperature
$T_{c\ Pt1000}$ – case temperature value measured by Pt 1000
T_j – junction temperature
T_{js} – junction temperature value obtained from the simulation
q – heat flux
ρ_d – air density
ρ_v – power density
U_{Tc} – total uncertainty of the case temperature measurement
(λ) – CIE photopic luminous efficiency function of the eye
V_F – forward voltage
V_{th} – threshold voltage

Table 1. The basic parameters of the tested diodes [23–26]; λ – the wavelength of the emitted radiation
Tabela 1. Podstawowe parametry badanych diod [14–17]; λ – długość fali emitowanego promieniowania

No.	Model	Manufacturer	Junction	Color	I_F	V_F	λ
					[mA]	[V]	[nm]
1	LUYF503F33	Wenrun	AlGaInP	yellow	20	1.8–2.2	593
2	LBG503E43	Wenrun	InGaN	green	20	2.9–3.5	503
3	LL-504BC2E-B4-2GD	Lucky Light	InGaN	blue	20	2.8–4.0	466
4	LL-504WC2V-W2-3QD	Lucky Light	InGaN	cold white	20	2.8–4.0	455

through the same junction. The concurrent flow of I_H and I_m through the diode junction allowed for a simplification of the measurement circuit. After a time period determined experimentally, the value of T_j stabilized. Once this time had passed, the I_H current was switched off. For the next 20 ms, only the I_m current flowed through the diode junction. It was assumed that during this short time, the T_j value remained close to the value just before switching off I_H, and based on the measurement of V_F, it was possible to determine the junction temperature T_j.

The described measurement circuit is shown in Figure 1.

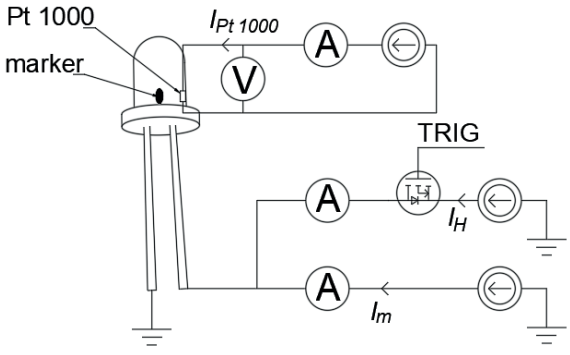

Fig. 1. A system of the indirect measurement of T_j based on the measurement of T_c and the known relationship $I_m = f(V_F)$. The T_c measurement is carried out using a Pt 1000 sensor and thermographic on a reference marker painted with Velvet Coating 811-21
Rys. 1. Układ pomiarowy do pośredniego termograficznego pomiaru temperatury złącza T_j na podstawie pomiaru temperatury obudowy T_c oraz zależności $I_m = f(V_F)$. Pomiar T_c wykonany za pomocą czujnika Pt 1000 oraz termograficznie — na markerze namalowanym farbą Velvet Coating 811-21

The measurement of the forward voltage drop V_F at the diode junction was performed when only the current I_m flowed through the junction. In this case, it was possible to use V_F as TSP, because prior to the measurements, the relationship $I_m = \mathrm{f}(V_F)$ was determined. For this purpose, all diodes were placed inside the chamber. The temperature inside the chamber was changed in the range from –8 °C to 70 °C. The current I_m flowed through the series-connected diodes. After each temperature setting, the experimentally determined time was allowed to pass until the measured value of V_F stabilized. It was assumed that after this time the temperature inside the chamber T_a was equal to T_j. The measurement scheme enabling the determination of the relationship $I_m = \mathrm{f}(V_F)$ is shown in Figure 2.

The thermographic imaging system and the diodes assembly were placed inside a custom-designed enclosure made of plexiglass, with the internal dimensions of 40 cm × 30 cm × 30 cm. The inner walls of the enclosure were lined with black polyurethane foam. Due to its open-cell structure, which mimics the

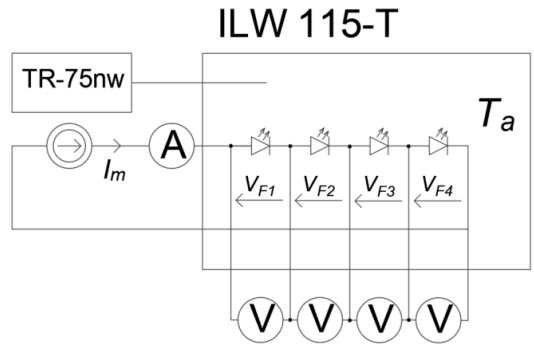

Fig. 2. A system used to determine the relationship $I_m = f(V_F)$. The measurement was carried out in an ILW 115-T chamber. The temperature measurement was performed using a TR-75nw device equipped with a type K thermocouple
Rys. 2. Układ do wyznaczenia zależności $I_m = f(V_F)$. Pomiar przeprowadzony w komorze ILW 115-T. Pomiar temperatury wykonano za pomocą TR-75nw wyposażonego w termoelement typu K

behavior of a blackbody cavity, this material exhibits a high emissivity value of approximately $\varepsilon = 0.94$ [14]. This design effectively shielded the measurement setup from external thermal influences and significantly reduced the internal reflections [15, 16].

To precisely adjust the distance d between the lens of the thermographic camera and the surface of the epoxy mold compound, the camera was mounted on a tripod integrated with a stepper motor. This motorized positioning system enabled the precise control of the distance d, managed by a Siemens S7-1200 1214DC/DC/DC programmable logic controller (Siemens, Munich, Germany) [29]. The desired distance was set using a Siemens KTP 700 Basic PN touchscreen interface [30]. An overview of the complete measurement setup is shown in Figure 3.

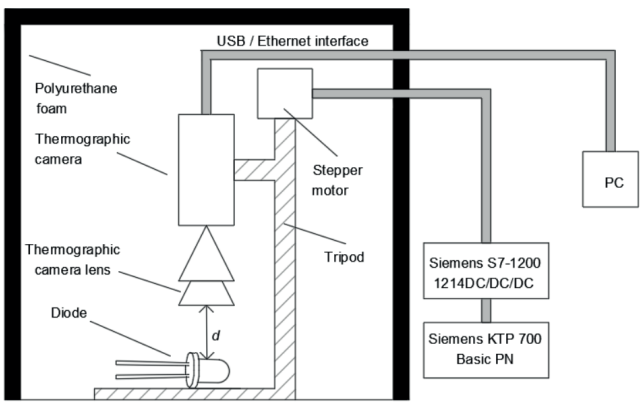

Fig. 3. The described measurement system
Rys. 3. Zastosowany układ pomiarowy

2.2. Finite element method and boundary conditions

In the subsequent phase of the indirect thermographic temperature assessment, the objective was to determine the correlation between the junction temperature (T_j) and the case temperature (T_c). This correlation can be determined using the numerical simulations. One of the applicable approaches is the Finite Element Method (FEM), in which the region of interest for evaluating the temperature distribution is discretized into a finite number of tetrahedral elements.

The heat transfer in the x-direction between two points is described by equation (1) [17].

$$-\rho_v = k \cdot \frac{\partial^2 T}{\partial x^2} - c_{th} \cdot \frac{\partial T}{\partial t} \tag{1}$$

where: ρ_v – the power density dissipated in the junction in W/m^3, c_{th} – the thermal capacity, T – the temperature, k – the thermal conductivity.

For steady-state conditions, the equation (1) reduces to the form presented in equation (2) [17].

$$q = -k \cdot \frac{dT}{dx} \tag{2}$$

where q denotes the heat flux, expressed in watts per square meter (W/m^2).

By using the separation of variables technique and integrating equation (2), the time constant can be determined after applying the boundary conditions defined in equation (3).

$$\begin{aligned} &\text{for} \quad x = 0 \rightarrow T = T_1 \\ &\text{for} \quad x = x_k \rightarrow T = T_2 \end{aligned} \tag{3}$$

After determining the time constant and assuming that the heat flux q has completely passed through the wall, equation (3) can be reformulated into the form shown in equation (4).

$$T_1 - T_2 = x_k \cdot \frac{P_c}{S \cdot k} \tag{4}$$

where P_c is the total power applied to the heat source in W and S in m^2 is the area of the wall penetrated by q in W/m^2.

For accurate FEM-based simulations, it is essential to determine both the radiation coefficient h_r and the convection coefficient h_c. The radiation coefficient h_r can be obtained from equation (5).

$$h_r = \sigma \cdot (T_c + T_a) \cdot (T_c^2 + T_a^2) \tag{5}$$

The convection coefficient h_c represents the rate of convective heat transfer per unit surface area over time. Its precise determination is complex, as it depends on various factors such as the geometry, the structural complexity and the surface temperature of the object participating in convection. In the present work, h_c was approximated using similarity theory in transport phenomena. The interrelations between the key physical parameters were expressed through dimensionless numbers, including the Nusselt, Grashof, and Prandtl numbers. For planar surfaces, h_c can be computed using the relationship given in equation (6) [18].

$$h_c = \frac{Nu \cdot k}{L} \tag{6}$$

The Nusselt number is expressed according to the formulation in equation (7) [32].

$$Nu = e(G_r \cdot P_r)^f \tag{7}$$

where e and f are dimensionless coefficients, the values of which depend on the shape and orientation of the analyzed surface and the product $P_r \cdot G_r$. P_r (—) is the Prandtl number, G_r is the Grashof number.

The values of the coefficients e_{lam}, e_{turb}, f_{lam}, and f_{turb} are influenced by the product of the Grashof and Prandtl numbers, along with the surface orientation and whether the airflow over the surface is laminar or turbulent. The specific coefficient values are listed in Table 2 [18].

The Prandtl number is determined using the expression given in Equation (8) [18].

$$P_r = \frac{c \cdot \psi}{k} \tag{8}$$

where c is the specific air heat equal to 1005 in J · kg^{-1} · K^{-1} in 293.15 K, ψ is the dynamic air viscosity equal to 1.75×10^{-5} in kg · m^{-1} · s^{-1} in 273.15 K.

The Grashof number is obtained from the formula presented in Equation (9) [18].

$$G_r = \frac{\alpha \cdot g \cdot (T_c - T_a) \cdot \rho_d^3 \cdot L^3}{\psi^2} \tag{9}$$

where α is a coefficient of the expansion equal to 0.0034 in K^{-1}, g is the gravitational acceleration of 9.8 in m · s^{-2}, ρ_d is the air density equal to 1.21 in kg · m^{-3} in 273.15 K.

Heating power P_h is the difference between the electrical power dissipated in the junction P_j and the optical power P_o — (equation 10).

$$P_h = P_j - P_o \tag{10}$$

Using the formula for determining LER (Luminous Efficacy of Radiation) given in [28], and taking into account that φ_e (radiant flux) = P_o, equation (11) one can derived:

$$P_o = \frac{\varphi_v}{LER} \tag{11}$$

where φ_v is the luminous flux, LER is the luminous efficacy of the radiation.

Based on the definition of luminous flux [29], equation (12) can be derived:

$$\varphi_v = I_v \cdot \omega \tag{12}$$

where I_v is the luminous intensity (cd), ω is the solid angle of the beam (sr).

The value of ω (equation 12) can be determined from the geometry of the solid angle of the cone. In this work, $\theta_{\frac{1}{2}}$ was

considered as the half-angle of the luminous flux divergence.

$$\omega = 2 \cdot \pi \cdot \left(1 - \cos \theta_{\frac{1}{2}} \right) \tag{13}$$

An approximate value of LER can be determined from equation (14) [19]:

$$LER = K_m \int_0^\infty B_\lambda V(\lambda) d\lambda \tag{14}$$

where B_λ is the normalized spectral power distribution, $V(\lambda)$ is the CIE photopic luminous efficiency function of the eye [33], K_m is the photopic luminous efficacy constant, equal to 683 (lm/W).

In the case of diodes emitting within a narrow wavelength range (quasi-monochromatic diodes), equation (14) can be simplified to the form of equation (15).

$$LER = 683 \cdot V(\lambda) \tag{15}$$

This is possible upon taking into account equation (16) [34]:

$$B_\lambda = \delta(\lambda - \lambda_0) \tag{16}$$

where: λ is the wavelength, λ_0 is the selected wavelength at which the energy is concentrated, $\delta()$ is Dirac delta.

Equation (15) does not hold for white diodes (e.g., row 5 in Table 1). Therefore, for this case the LER value was adopted from the literature [20].

Consequently, it is possible to determine the value of the optical efficiency η_o – equation (17) expressed as a the ratio P_o to P_j. [21].

$$\eta_o = \frac{P_o}{P_j} \tag{17}$$

3. Results

At the beginning of the conducted study, using the setup shown in Figure 2, the V_F values were measured for each of the four LEDs. The obtained results are presented in Table 3.

Next, assuming that under steady-state conditions $T_a = T_j$, the relationships $T_j = f(V_F)$ were determined for each diode. The obtained dependencies are presented in Table 4.

The next stage of the work involved creating a three-dimensional model of the diode. SolidWorks software (Dassault Systèmes SolidWorks Corp, Vélizy-Villacoublay, France) was used for this purpose. In order to create the model, it was necessary to dimension the internal structure of the diode and assign thermal conductivity values k to its individual materials. The values of the thermal conductivity parameters k assigned to the specific components of the diode are presented in Table 5.

Table 2. Values of the coefficients e_{lam}, e_{turb}, f_{lam}, and f_{turb}
Tabela 2. Wartości współczynników e_{lam}, e_{turb}, f_{lam}, oraz f_{turb}

Shape	$G_r P_r$	e_{lam}	f_{lam}	e_{turb}	f_{turb}
Vertical flat wall	10^9	0.59	0.25	0.129	0.33
Upper flat wall	10^8	0.54	0.25	0.14	0.33
Lower flat wall	10^5	0.25	0.25	NA	NA

Table 3. Values enabling the determination of the relationship $I_m = f(V_F)$
Tabela 3. Wartości umożliwiające wyznaczenie zależności $I_m = f(V_F)$

I_m	T_a	$V_{F\_LUYF503F33}$	$V_{F\_LBG503E43}$	$V_{F\_LL-504BC2E}$	$V_{F\_LL-504WC2V}$
[µA]	[°C]	[V]	[V]	[V]	[V]
100	–8.1	1.837	2.40	2.47	2.55
100	0.6	1.813	2.38	2.46	2.54
100	10.3	1.789	2.36	2.45	2.53
100	19.9	1.777	2.32	2.43	2.51
100	30.2	1.750	2.30	2.42	2.50
100	38.5	1.736	2.28	2.41	2.49
100	49.6	1.712	2.26	2.40	2.47
100	59.5	1.689	2.25	2.38	2.46
100	67.3	1.670	2.23	2.37	2.45

Table 4. Obtained relationships $T_j = f(V_F)$
Tabela 4. Uzyskane zależności $T_j = f(V_F)$

No.	LED model	Determined relationship
1	LUYF503F33	$T_j = -464.87 \cdot V_F + 844.46$
2	LBG503E43	$T_j = -432.00 \cdot V_F + 1027.2$
3	LL-504BC2E	$T_j = -734.41 \cdot V_F + 1807.0$
4	LL-504WC2V	$T_j = -734.41 \cdot V_F + 1865.8$

Before starting the simulation, the appropriate edge length of the finite element was determined. The optimal size was assumed to be the one that minimizes simulation time while ensuring stable results. The achieved results are presented in Table 6.

A mesh based on the mixed curvature was used. The maximum element size was 0.25 mm, while the minimum size was 0.05 mm. The mesh contained 126 788 nodes and 84 018 elements.

An example model created in SolidWorks and the simulation result are shown in Figure 4.

Thermal measurements were then performed. The example thermograms are presented in Figures 5 and 6.

Subsequently, measurements were carried out using the systems shown in Figures 3 and 1. The measured values of the current I_H flowing through the diode, the calculated electrical power dissipated in the diode junction P_j based on the measured voltage V_F and current I_F (electrical power), the temperature measured using the thermographic camera $T_{c\ cam}$, the

Table 5. Materials Used During the Simulation and the Corresponding Thermal Conductivity Coefficients (k-values)
Tabela 5. Materiały użyte podczas symulacji oraz odpowiadające im współczynniki przewodnictwa cieplnego (wartości *k*)

No.	Part of the diode	Material	k [W/m · K]
1	Junction	Silicon	124
2	External legs	Copper	390
3	Internal leads	Copper	390
4	Transparent case	Melamine resin	0.272

Table 6. Edge size of the mesh element and the corresponding simulation time
Tabela 6. Wymiar krawędzi elementu siatki oraz odpowiadający mu czas symulacji

No.	Mesh element edge lenght	Simulation time	Δ_{Tc}s
	[mm]	[s]	[°C]
1	0.25	22.0	0.05
2	0.50	2.0	0.10
3	0.75	1.5	0.20
4	1.00	1.0	0.20
5	1.50	0.5	0.30

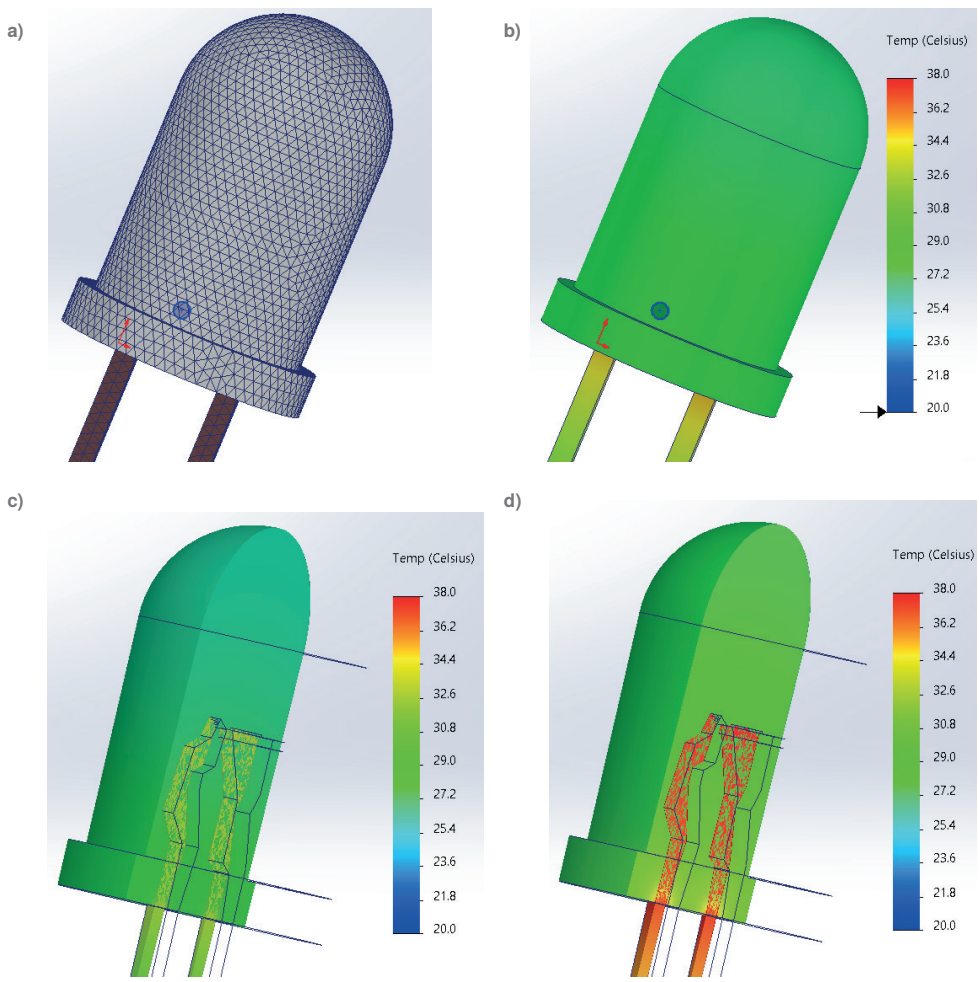

Fig. 4. a) Example model created in SolidWorks (with mesh and measurement point); b) the result of an example simulation for T_j = 33.3 °C, T_{cs} = 28.9 °C, with measurement point; c) the result of the simulation for T_{cs} = 28.1 °C; d) the result of the simulation for T_{cs} = 29.9 °C
Rys. 4. a) Model utworzony w programie SolidWorks (z siatką i punktem pomiarowym); b) wynik symulacji dla T_j = 33,3 °C, T_{cs} = 28,9 °C z punktem pomiarowym; c) wynik symulacji dla T_{cs} = 28,1 °C; d) wynik symulacji dla T_{cs} = 29,9 °C

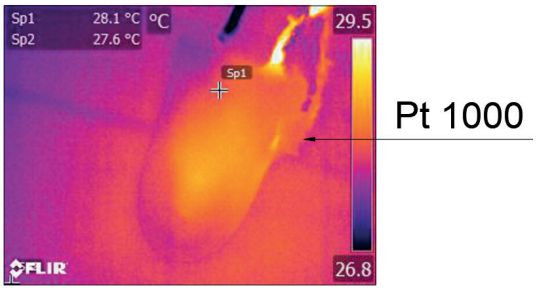

Fig. 5. An example thermogram of a diode, T_c = 28.1 °C
Rys. 5. Termogram diody dla T_c = 28,1 °C

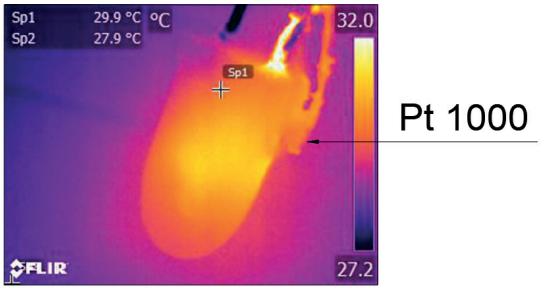

Fig. 6. An example thermogram of a diode, T_c = 29.9 °C
Rys. 6. Termogram diody dla T_c = 29,9 °C

Table 7. The results obtained for the diode LUYF503F33. The estimated value of η_o was 0.03
Tabela 7. Wyniki dla diody LUYF503F33. Szacowana wartość η_o = 0,03

I_F	V_F	P_j	$T_{c\ cam}$	$\Delta_{grTccam}$	$T_{c\ Pt1000}$	$\Delta_{grTcPt1000}$	U_{Tc}	T_j	T_{cs}	T_{js}
[mA]	[V]	[W]	[°C]	[°C]	[°C]	[°C]	[°C]	[°C]	[°C]	[°C]
4.9	1.89	0.0093	27.1	2	25.6	0.43	1.94	28.4	27.6	28.0
9.8	1.98	0.0194	28.8	2	26.3	0.43	1.94	32.1	29.0	31.7
14.8	2.03	0.0300	30.5	2	27.2	0.44	1.94	35.4	30.9	34.9
19.7	2.07	0.0408	31.9	2	28.1	0.44	1.95	39.2	32.2	38.7
24.8	2.12	0.0526	33.1	2	29.1	0.45	1.95	43.2	33.5	43,0
29.7	2.26	0.0642	35.1	2	30.2	0.45	1.95	46.1	35.5	45.9

Table 8. The results obtained for the diode LBG503E43. The estimated value of η_o was 0.04
Tabela 8. Wyniki dla diody LBG503E43. Szacowana wartość η_o = 0,04

I_F	V_F	P_j	$T_{c\ cam}$	$\Delta_{grTccam}$	$T_{c\ Pt1000}$	$\Delta_{grTcPt1000}$	U_{Tc}	T_j	T_{cs}	T_{js}
[mA]	[V]	[W]	[°C]	[°C]	[°C]	[°C]	[°C]	[°C]	[°C]	[°C]
4.9	2.70	0.0132	24.1	2	23.1	0.42	1.94	25.9	24.3	25.7
9.8	2.95	0.0289	27.5	2	26.2	0.43	1.94	31.5	27.8	31.1
14.8	3.08	0.0456	30.3	2	28.3	0.44	1.95	37.1	30.5	36.7
19.7	3.18	0.0626	31.7	2	29.9	0.45	1.95	41.0	31.9	40.6
24.8	3.26	0.0808	33.8	2	31.9	0.46	1.95	45.7	34.1	45.0
29.7	3.33	0.0989	36.5	2	34.0	0.47	1.95	50.1	36.9	49.5

Table 9. The results obtained for the diode LL-504BC2E. The estimated value of η_o was 0.29
Tabela 9. Wyniki dla diody LL-504BC2E. Szacowana wartość η_o = 0,29

I_F	V_F	P_j	$T_{c\ cam}$	$\Delta_{grTccam}$	$T_{c\ Pt1000}$	$\Delta_{grTcPt1000}$	U_{Tc}	T_j	T_{cs}	T_{js}
[mA]	[V]	[W]	[°C]	[°C]	[°C]	[°C]	[°C]	[°C]	[°C]	[°C]
4.9	2.55	0.0125	27.3	2	–	–	1.90	28.4	27.5	28.0
9.8	2.67	0.0262	28.1	2	–	–	1.90	31.9	28.4	31.2
14.8	2.76	0.0408	29.6	2	–	–	1.90	34.8	30.0	34.0
19.7	2.85	0.0561	31.2	2	–	–	1.90	39.3	31.4	38.6
24.8	2.92	0.0724	32.9	2	–	–	1.90	43.6	33.2	43.0
29.7	2.99	0.0888	34.8	2	–	–	1.90	47.8	35.2	47.1

Table 10. The results obtained for the diode LL-504WC2V. The estimated value of η_o was 0.05
Tabela 10. Wyniki dla diody LL-504WC2V. Szacowana wartość η_o = 0,05

I_F	V_F	P_j	$T_{c\ cam}$	$\Delta_{grTc\,cam}$	$T_{c\ Pt1000}$	$\Delta_{grTc\,Pt1000}$	U_{Tc}	T_j	T_{cs}	T_{js}
[mA]	[V]	[W]	[°C]	[°C]	[°C]	[°C]	[°C]	[°C]	[°C]	[°C]
4.9	2.66	0.0130	27.3	2	–	–	1.90	28.5	27.6	28.2
9.8	2.81	0.0275	28.6	2	–	–	1.90	31.8	29.0	31.6
14.8	2.91	0.0431	30.0	2	–	–	1.90	36.0	30.3	35.7
19.7	3.00	0.0591	31.7	2	–	–	1.90	40.3	32.0	39.9
24.8	3.07	0.0761	33.4	2	–	–	1.90	44.9	33.8	44.3
29.7	3.13	0.0930	35.1	2	–	–	1.90	48.3	35.7	47.8

junction temperature determined from the obtained function $T_j = f(V_F)$, the case temperature measured using the Pt 1000 sensor $T_{c\ Pt1000}$, and the junction temperature T_{js} and the case temperature T_{cs} of the diode obtained from the simulation results are presented in Tables 7–10.

4. Conclusion and discussion

The operating temperature of the junction in light-emitting diodes (LEDs) is a key parameter for ensuring their proper operation. Its value provides important information about the operating conditions; however, direct measurement during normal operation is practically impossible. A solution to this problem is the use of an indirect method that enables the measurement of junction temperature. In this method, the junction temperature can be determined based on the thermographic measurement of the case temperature and a relationship linking it to the junction temperature. In the conducted research, this relationship between these two temperatures was determined using simulation methods in SolidWorks software.

The main objective of the research presented in the article was to demonstrate that, based on a thermographic measurement of the case temperature and supported by simulation studies, it is possible to obtain a reliable estimation of the junction temperature. Additionally, the conducted simulations enabled the determination of the internal temperature distribution within the tested diodes, which made it possible to identify the most optimal measurement point, where the difference between the case temperature and the junction temperature is the smallest.

In order to carry out the simulations, it was necessary to measure the internal dimensions of the tested diodes and to determine the thermal conductivity coefficients of the materials from which the diodes were made. The reliability of the constructed model and the selected parameters, and consequently, the simulation results, was confirmed through thermographic measurements and the electrical method. The thermographic measurements made it possible to verify the case temperature obtained from the simulations, while the electrical method was used to verify the junction temperature. Additionally, the case temperature results were validated using a Pt 1000 temperature sensor. As a result of the conducted comparisons, it was observed that the discrepancies did not exceed the measurement uncertainty of the instruments used.

During the modelling process, the diode's optical efficiency was taken into account. This approach allowed for a more realistic representation of the component's operating conditions, reflecting the actual energy balance between the thermal losses and optical emission. An approximate method was used, based on values from datasheets and literature. In the calculations, the value of the power dissipated in the junction was considered for the forward current closest to 20 mA. The results obtained with the proposed method provide only approximate values of optical efficiency. To determine more accurate values, direct measurements should be performed.

Based on the obtained results, it can be concluded that by combining the simulation method with thermographic measurements, it is possible to perform an indirect measurement of the junction temperature of LED diodes. The analysis of thermograms and simulation results confirmed these findings for different power levels dissipated at the junctions of the tested LED diodes.

Bibliography

1. Chhajed S, Xi Y., Gessmann Th., Xi Y.-Q., Shah J.M., Kim J.K., Schubert E.F., *Junction temperature in light--emitting diodes assessed by different methods*, Proceedings of SPIE, Vol. 5739, 2005, DOI: 10.1117/12.593696.
2. Vaskuri A., Kärhä P., Baumgartner H., Kantamaa O., Pulli T., Poikonen T., Ikonen E., *Relationships between junction temperature, electroluminescence spectrum and ageing of light-emitting diodes*, "Metrologia", Vol. 55, No. 2, 2018, 86–95, DOI: 10.1088/1681-7575/aaaed2.
3. Dziarski K, Hulewicz A, Kuwałek P, Wiczyński G., *Methods of Measurement of Die Temperature of Semiconductor Elements: A Review*, "Energies", Vol. 16, No. 6, 2023, DOI: 10.3390/en16062559.
4. Cengiz C., Azarifar M., Arik M., *A Critical Review on the Junction Temperature Measurement of Light Emitting Diodes*, "Micromachines", Vol. 13, No. 10, 2022, DOI: 10.3390/mi13101615.
5. Więcek B., De Mey G., *Thermovision in Infrared–Basics and Applications*, Measurement Automation Monitoring Publishing House: Warszawa, Poland, 2011.
6. Minkina W., *Pomiary termowizyjne – przyrządy i metody.* Wydawnictwo Politechniki Częstochowskiej, Częstochowa 2004, ISBN 83-7193-237-5.
7. Hulewicz A., Dziarski K., Dombek G., *The Solution for the Thermographic Measurement of the Temperature of a Small Object*, "Sensors", Vol. 21, No. 15, 2021, DOI: 10.3390/s21155000.
8. Chang K.S., Yang S.C., Kim J.-Y., Kook M.H., Ryu S.Y., Choi H.Y., Kim G.H., *Precise Temperature Mapping of GaN-Based LEDs by Quantitative Infrared Micro-Thermography*, "Sensors", Vol. 12, No. 4, 2012, 4648–4660, DOI: 10.3390/s120404648.

9. Cheng H-Ch., Lin J.-Y., Chen W.-H., *On the thermal characterization of an RGB LED-based white light module*, "Applied Thermal Engineering", Vol. 38, 2012, 105–116, DOI: 10.1016/j.applthermaleng.2012.01.014
10. Lee D., Choi H., Jeong S., Jeon C.H., Lee D., Lim J., Byon C., Choi J., *A study on the measurement and prediction of LED junction temperature*, "International Journal of Heat and Mass Transfer", Vol. 127 (B), 2018, 1243–1252, DOI: 10.1016/j.ijheatmasstransfer.2018.07.091.
11. JM Lasance C., Poppe A., *Thermal Management for LED Applications*, Springer, 2014, DOI: 10.1007/978-1-4614-5091-7.
12. Rongier C., Gilblas R., Le Maoult Y., Belkessam S., Schmidt F., *Infrared thermography applied to the validation of thermal simulation of high luminance LED used in automotive front lighting*, "Infrared Physics & Technology", Vol. 120, 2022, DOI: 10.1016/j.infrared.2021.103980.
13. Tang-Kwor E., Mattei S., *Emissivity measurements for nextel velvet coating 811-21 between – 36 °C and 82 °C*, 15th European Conference on Thermophysical Properties, Vol. 33, 1999, 551–556.
14. Baillis D., Coquard R., Randrianalisoa J.H., Dombrovsky L.A., Viskanta R., *Thermal radiation properties of highly porous cellular foams*, "Special Topics & Reviews in Porous Media: An International Journal", Vol. 4, No. 2, 2013, 111–136, DOI: 10.1615/SpecialTopicsRevPorousMedia.v4.i2.20.
15. Minkina W., Dudzik S., *Infrared Thermography Errors and Uncertainties*, John Wiley & Sons, 2009, DOI: 10.1002/9780470682234.
16. Więcek B., *Thermovision in infrared – basic and applications*. Measurement Automotion Monitoring Publish House, Warszawa 2011.
17. Kopeć M., Więcek B., *AC temperature estimation of power electronic devices using 1D thermal modeling and IR thermography measurements*. 15th Quantitative InfraRed Thermography Conference, 2020, DOI: 10.21611/qirt.2020.161.
18. Dziarski H., Hulewicz A., Dombek G., Drużyński Ł., *Indirect Thermographic Temperature Measurement of a Power-Rectifying Diode Die*, "Energies", Vol. 15, No. 9, 2022, DOI: 10.3390/en15093203
19. Murphy T.W. Jr., *Maximum Spectral Luminous Efficacy of White Light*, "Journal of Applied Physics", Vol. 111, No. 10, 2012, DOI: 10.1063/1.4721897.
20. Ohno Y., *Spectral design considerations for white LED color rendering*, "Optical Engineering", Vol. 44, No. 11, 2005, DOI: 10.1117/1.2130694.
21. Tsonev D., Videv S., Haas H., *Light fidelity (Li-Fi): Towards all-optical networking*, "Optics Express", Vol. 25, No. 16, 2017, 18990–19005, DOI: 10.1117/12.2044649.

Inne źródła

22. JEDEC, Integrated Circuit Thermal Measurement Method – Electrical Test Method, [www.jedec.org/standards-documents/docs/jesd-51-1]
23. Wenrun Optoelectronic, LUY503F33 LED, [www.tme.eu/Document/69a3a40f1e4d84664d-729c511a6bcff7/LUY503F33.pdf].
24. Lucky Light Electronics, LL-504BC2E-B4-2GD LED, [www.tme.eu/Document/37f277d817111bf24ddd39ea1d2d-dfc4/LL-504BC2E-B4-2GD.pdf].
25. Wenrun Optoelectronic, LBG503E43 LED, [www.tme.eu/Document/6fd9e9e74a82e6fab8cd4b-fabe020323/LBG503E43.pdf].
26. Lucky Light Electronics, LL-504WC2V-W2-3QD LED, [www.tme.eu/Document/71c2f42910d8d1d1bd5d8a-ca92a7164d/ll-504wc2v-w2-3qd.pdf].
27. TME, Platinum Temperature Sensor Pt 1000-550, [www.tme.eu/Document/67cf717905f835bc5efcdcd-56ca3a8e2/Pt1000-550_EN.pdf].
28. https://www.tme.eu/Document/7a228d9a81f73f75bba-8707a2357bb2d/WLK_DTE.pdf
29. PLC Controller. Available online: https://docs.rs-online.com/4ed5/0900766b81397276.pdf
30. HMI Panel. Available online: https://static.rapidonline.com/pdf/543842_v1.pdf
31. https://cie.co.at/eilvterm/17-21-090 (available online: 16.09.2025)
32. https://cdn.standards.iteh.ai/samples/102846/0802d-0f5a29d49018f588cc18565f2ba/ISO-80000-7-2019.pdf
33. https://cie.co.at/datatable/cie-spectral-luminous-efficiency-photopic-vision
34. https://bklein.ece.gatech.edu/laser-photonics/monochromaticity-the-spectrum-of-a-laser-or-other-light-source/?utm

Pomiar temperatury złącza diod elektroluminescencyjnych (LED) na podstawie termograficznego pomiaru temperatury obudowy

Streszczenie: W artykule opisano użycie pośredniego pomiaru termowizyjnego do wyznaczenia temperatury złącza wybranych diod elektroluminescencyjnych (LED). Przedstawiono metodę pomiaru umożliwiającą wiarygodną ocenę tej temperatury oraz zastosowaną w pracach symulacyjnych metodę elementów skończonych (MES). Omówiono proces wyznaczania wartości współczynników niezbędnych do przeprowadzenia symulacji. Zaprezentowano wyniki badań symulacyjnych wykonanych w środowisku SolidWorks, pomiary termograficzne temperatury obudowy badanych diod LED oraz odpowiadające im oszacowane wartości temperatury złącza. Wiarygodność uzyskanych wyników potwierdzono metodą elektryczną oraz pomiarami z wykorzystaniem czujnika Pt 1000.

Słowa kluczowe: termografia, dioda elektroluminescencyjna, metrologia

Arkadiusz Hulewicz, PhD Eng.

arkadiusz.hulewicz@put.poznan.pl
ORCID: 0000-0001-9342-7430

A graduate of the Faculty of Electrical Engineering at the Poznan University of Technology, where he has been employed since 2001. Currently an assistant professor and academic teacher in the Department of Metrology of Electronics and Light Technology. Author and co-author of 93 publications. His main scientific interests are metrology, the thermographic measurements, the bio--measurements and the biomedical engineering, the optoelectronics, as well as modeling and signal processing, especially the thermal modelling.

Krzysztof Dziarski, PhD Eng.

krzysztof.dziarski@put.poznan.pl
ORCID: 0000-0002-7877-4116

Assistant Professor at the Institute of Electric Power Engineering, Poznań University of Technology. He obtained a PhD in technical sciences with a specialization in electrical engineering, focusing on advanced methods of thermal diagnostics in electronic systems. His doctoral dissertation concerned the application of infrared thermography and numerical simulations to analyze heat dissipation in semiconductor components. His research interests include thermal management, thermographic diagnostics, and reliability analysis of electronic components. He actively participates in scientific projects and teaching activities, supervising engineering and master's theses in the field of temperature measurement techniques, electronics, and residential electrical installations.